# Drude weight in hard-core boson systems: Possibility of a finite-temperature ideal conductor

Gourab Majumder and Arti Garg
*Condensed Matter Physics Division, Saha Institute of Nuclear Physics, 1/AF Bidhannagar, Kolkata 700 064, India*
(Received 16 February 2016; revised manuscript received 13 September 2016; published 12 October 2016)

We calculate the Drude weight in the superfluid (SF) and supersolid (SS) phases of the hard-core boson (HCB) model on a square lattice using stochastic series expansion (SSE). We demonstrate from our numerical calculations that the normal phase of HCBs in two dimensions can be an *ideal conductor* with dissipationless transport. In two dimensions, when the ground state is a SF, the superfluid stiffness drops to zero with a Kosterlitz-Thouless type transition at $T_{\rm KT}$. The Drude weight, though is equal to the stiffness below $T_{\rm KT}$, surprisingly, stays finite even for a range of temperatures above $T_{\rm KT}$ indicating the nondissipative transport in the normal state of this system. In contrast to this, in a three-dimensional SF phase, where the superfluid stiffness goes to zero continuously via a second-order phase transition at $T_c$, the Drude weight goes to zero at $T_c$, as expected. We also calculated the Drude weight in a two-dimensional SS phase, where the charge density wave (CDW) order coexists with superfluidity. For the SS phase we studied, superfluidity is lost via a Kosterlitz-Thouless transition at $T_{\rm KT}$ and the transition temperature for the CDW order is larger than $T_{\rm KT}$. In striped SS phase where the CDW order breaks the rotational symmetry of the lattice, the system behaves like an ideal conductor for a range of temperatures above $T_{\rm KT}$ along the lattice direction parallel to the stripes, while along the direction perpendicular to the stripes it behaves like an insulator for all $T > T_{\rm KT}$. In contrast to this, in the star-SS phase, the Drude weight along both lattice directions goes to zero along with the superfluid stiffness and for $T > T_{\rm KT}$ we have the finite temperature phase of a CDW insulator.

DOI: 10.1103/PhysRevB.94.134508

## I. INTRODUCTION

The superfluid phase of bosons is a canonical quantum fluid just like the Fermi liquid phase of fermions. One of the frontiers of quantum condensed matter physics is to explore quantum phases of bosons in two dimensions that are not superfluids. Lattice models of interacting bosons in two dimensions, such as the Bose-Hubbard model, which have been studied in the past, primarily as models for Josephson junction arrays [1] and in the context of optical lattice experiments [2] and hard-core bosons, which have been studied in the context of the pseudogap phase of high-$T_c$ superconductors [3], are known to have insulating and superfluid phases [4,5]. In some cases, the coexistence of charge density wave (CDW) order and superfluidity, which is known as the supersolid (SS) phase, is also seen [5–11]. The most challenging phase, which is rarely seen, is a gapless, compressible "Bose-metal" phase, which breaks no symmetry whatsoever. There are very few examples of studies [12–15] where the "Bose-metal" phase has been realized.

Following Scalapino *et al.* [16], a superfluid (SF) phase is the one in which both superfluid stiffness $\rho_s$ and the Drude weight $D$ are nonzero. In an insulating phase, e.g., in the CDW ordered phase, both $\rho_s = D = 0$. Here, $D$ is the delta function part of the charge conductivity $\sigma(\omega) = D\delta(\omega) + \sigma_{\rm reg}(\omega)$ and $\rho_s$ is given by the curvature of the thermodynamic limit of the free energy ($\sim d^2F/d\phi^2$) with respect to a twist in boundary conditions ($\phi$). Conventionally, in a charged superfluid or a superconductor, $D$ remains nonzero not only at zero temperature but for all temperatures below the transition temperature and is believed to be zero for temperatures above the transition temperature. In contrast to this, in a metal only at $T = 0$, the Drude weight is nonzero. With increase in temperature, the $\delta(\omega)$ peak in the conductivity gets broadened due to thermal fluctuations resulting in zero Drude weight. In this context, it is interesting to consider noninteracting Bose gas in one and two dimensions. In this case, at any finite temperature, $\rho_s = 0$ but since the current operator commutes with the Hamiltonian, the Drude weight remains finite at finite temperature. Therefore noninteracting bosons in one and two dimensions at finite temperature are "trivial" examples of *ideal conductors* [17]. In this paper, we explore the possibility of having a dissipationless ideal conductor of interacting bosons where $\rho_s$ goes to zero at certain transition temperature but $D$ remains nonzero for a range of temperatures above the transition temperature.

To be specific, in this paper, we study the Drude weight in a model of hard-core bosons (HCB), with nearest- and next-nearest-neighbor hopping and repulsion terms, on 2D square and cubic lattices. The phase diagram for this model of HCBs has been studied for a large range of parameters [4,5,8,9,11], but to the best of our knowledge, the Drude weight has not been calculated. We calculate the Drude weight in the SF, insulating, and the SS phases of this model using the stochastic series expansion method [18,19]. We demonstrate from our numerical calculations that the normal phase of HCBs in two dimensions can be an ideal conductor with dissipationless transport for a range of temperature near $T_{\rm KT}$. Before going to the details of the paper, we summarize our main results below.

In the two-dimensional case, for the SF ground state, the superfluid stiffness drops to zero in the thermodynamic limit via a Kosterlitz-Thouless [20] type transition at $T_{\rm KT}$ [4,21,22]. We show that though the Drude weight is equal to the stiffness below $T_{\rm KT}$, as expected, surprisingly, it remains finite even for a range of temperatures above $T_{\rm KT}$ indicating the presence of an ideal Bose conductor with nondissipative transport in the normal phase of this two-dimensional SF. On the other hand, in three dimensions, where the superfluidity is accompanied by the appearance of a true long-range order and the superfluid stiffness goes to zero via a continuous transition [23,24] at $T_c$, the Drude weight also goes to zero at $T_c$.

 

We also calculated the Drude weight in SS phases on a 2D square lattice. In spite of the long-range Ising order coexisting with superfluidity, $\rho_s$ drops to zero at $T_{\rm KT}$ via a Kosterlitz-Thouless type transition. One of the SS phases we studied has striped CDW order. In this case, along the direction perpendicular to the stripes (see Fig. 13) $D = \rho_s$ at all temperatures due to a spectral gap in the system and both $D$ and $\rho_s$ are zero above $T_{\rm KT}$. Along the lattice direction parallel to the stripes, $D$ remains finite even for $T > T_{\rm KT}$ near $T_{\rm KT}$. Therefore, for a range of temperature above $T_{\rm KT}$, the system is an ideal conductor along the direction parallel to the stripes, while it is a finite temperature insulator along the direction perpendicular to the stripes for all $T > T_{\rm KT}$. In the other SS phases we have studied, the CDW order exists in both lattice directions. Therefore along both directions, $D = \rho_s$ at all temperatures, and both quantities go to zero simultaneously at $T_{\rm KT}$.

The rest of this paper is organized as follows. In Sec. I, we present details of the model and the method used. Section II describes in detail the benchmarks on the code for the calculation of the Drude weight showing comparison with earlier published results and with exact diagonalization results on small system sizes. Section III describes the results in the CDW and the SF phases on a 2D square lattice followed up by our results for the SF phase on a 3D cubic lattice in Sec. IV. In Sec. V, we present results for the SS phases on a 2D square lattice. We end this paper with conclusions and discussions on our work.

## II. MODEL AND METHOD

We study hard-core bosons on a square lattice described by the following Hamiltonian:

$$H = -t\sum_{<ij>}(c_i^\dagger c_j + c_j^\dagger c_i) - t'\sum_{<<ij>>}(c_i^\dagger c_j + c_j^\dagger c_i) + V_1\sum_{<ij>} n_i n_j + V_2\sum_{<<ij>>} n_i n_j - \mu\sum_i n_i. \quad (1)$$

Here, $t$ is the hopping amplitude from site $i$ to its nearest-neighbor site, $\mu$ is the chemical potential, $t'$ is the next-nearest-neighbor hopping amplitude, and $V_1/V_2$, are the nearest-neighbor and next-neighbor repulsion terms, respectively. This model can be mapped onto the $S = \frac{1}{2}$ spin model using the exact mapping $S_i^\dagger = c_i^\dagger$ and $S_i^z = n_i - 1/2$. In the spin language, one gets the extended XXZ model:

$$H = -t\sum_{<ij>}(S_i^\dagger S_j^- + S_j^\dagger S_i^-) - t'\sum_{<<ij>>}(S_i^\dagger S_j^- + S_j^\dagger S_i^-) + V_1\sum_{<ij>} S_i^z S_j^z + V_2\sum_{<<ij>>} S_i^z S_j^z - h\sum_i S_i^z, \quad (2)$$

where $h = \mu - 2V_1 - 2V_2$. This model has been studied earlier extensively using stochastic series expansion. With only nearest-neighbor terms, this model is known to have an SF phase and an insulating phase with a CDW order. The quantum phase transition from SF to CDW phase can be attained either by tuning the repulsion term or the chemical potential [4,5]. The finite temperature phase diagram for this model has also been studied [4]. Upon increasing temperature, the superfluid stiffness drops to zero with a Kosterlitz-Thouless (KT) type transition at $T_{\rm KT}$, just like in the model with only nearest-neighbor hopping for the hard-core bosons [21,22]. On the other hand, in three dimensions, the superfluid transition is accompanied by the appearance of true long-range order and the superfluid stiffness goes to zero with a continuous transition [23,24]. The full model with next-neighbor interactions is known to have exotic supersolid phases [8–11]. In this paper, we study transport properties, mainly the Drude weight in the charge conductivity, of all these phases at finite temperature using SSE with a directed loop update [18]. Below, we describe how the Drude weight and superfluid stiffness can be calculated within linear response theory (Kubo formula) using SSE.

### Drude weight and superfluid stiffness

Superfluid stiffness ($\rho_s$) is given by the curvature of the thermodynamic limit of the free energy ($\pi/Nd^2F/d\phi^2$) with respect to a twist in boundary conditions ($\phi$). To evaluate it within SSE, we use the Kubo formula representation of this quantity [16]:

$$\rho_s = \langle -K_x\rangle - {\rm Re}\Lambda_{xx}(q_x = 0, q_y \to 0, i\omega_m = 0) = \frac{\langle W^2\rangle}{\beta}. \quad (3)$$

Here, $\langle -K_x\rangle$ is the kinetic energy, $\Lambda_{xx}(\vec{q}, i\omega_m)$ is the current current correlation function, and $\langle W^2\rangle$ is the winding number. Note that in this work, we will calculate and present results for the superfluid stiffness $\rho_s$, which is related to the superfluid density $n_s$ as $\rho_s = 2tn_s$.

For the model with nearest- and next-nearest-neighbor hopping, $K_x$ and the current operator $J_x$ are given by

$$K_x = -t\sum_i (c_i^\dagger c_{i+\hat{x}} + c_{i+\hat{x}}^\dagger c_i) - t'\sum_i (c_i^\dagger c_{i+\hat{x}\pm\hat{y}} + c_{i+\hat{x}\pm\hat{y}}^\dagger c_i), \quad (4)$$

$$J_x(q = 0) = it\sum_i (c_i^\dagger c_{i+\hat{x}} - c_{i+\hat{x}}^\dagger c_i) + it'\sum_i (c_i^\dagger c_{i+\hat{x}\pm\hat{y}} - c_{i+\hat{x}\pm\hat{y}}^\dagger c_i). \quad (5)$$

Here, $\hat{x}$ and $\hat{y}$ denote unit vectors along the $X$ and $Y$ axes of the lattice, respectively.

The Drude weight $D$ is obtained by taking the transport limit of the Kubo formula [16,25], namely,

$$D = \langle -K_x\rangle - \Lambda_{xx}(q_x = 0, q_y = 0, \omega \to 0). \quad (6)$$

Here, $\Lambda_{xx}$ is the current-current response function

$$\Lambda_{xx}(\vec{q}, i\omega_m) = \int_0^\beta d\tau e^{i\omega_m\tau}\langle J_x(\vec{q},\tau)J_x(-\vec{q},0)\rangle \quad (7)$$

and $\omega_m = 2\pi mT$ is the Matsubara frequency where $m$ is any integer.

To evaluate this expression within SSE, let us use the symbol $H_b^+$ for $c_b^\dagger c_{b+\hat{x}}$. Then $\Lambda_{xx}(\tau)$ is nothing but the imaginary-time ($\tau$) ordered average of the product $\langle H_{b_1}^{\sigma_1}(\tau)H_{b_2}^{\sigma_2}(\tau =$

0)⟩ where $b_1$ and $b_2$ are bond indices and $\sigma_{1,2} = \pm$ [26]. Within SSE, the time ordered average of any two such local operators [19] can be represented as follows:

$$\left\langle H^{\sigma_2}_{b_2}(\tau) H^{\sigma_1}_{b_1}(0) \right\rangle = \frac{\sum_k \sum_{n,m} \frac{(\tau-\beta)^n(-\tau^m)}{n!m!} < \Psi_k \left| H^n H^{\sigma_2}_{b_2} H^m H^{\sigma_1}_{b_1} \right| \Psi_k >_W}{Z} = \left\langle \sum_{m=0}^{n_s-2} \frac{(\beta-\tau)^n(\tau^m)}{\beta^n} \frac{(n-1)!}{(n-m-2)!m!} N^{\sigma_1\sigma_2}_{b_1 b_2}(m) \right\rangle_W , \quad (8)$$

where we have summations over $n$ and $m$ coming out from the Taylor expansion of $e^{(-\beta+\tau)H}$ and $e^{-\beta H}$ and $N^{\sigma_1\sigma_2}_{b_1,b_2}(m)$ is the number of times such a combination with $m$ nonidentity operators in between, appears in the operator sequence in SSE. The Fourier transform of Eq. (8) from $\tau$ to Matsubara frequency $\omega_m$ yields

$$\frac{-1}{\beta} \sum_{\sigma_1,\sigma_2=\pm} \sigma_1\sigma_2 \sum_m F^1_1(m+1, n_s; 2i\pi n) N^{\sigma_1\sigma_2}_{b_1 b_2}(m), \quad (9)$$

where $F^1_1$ is the confluent hypergeometric function of first order [26].

After calculating the current-current correlation function $\Lambda_{xx}(q, i\omega_n)$ this way within SSE, one calculates the Drude weight using Eq. (6). The analytical continuation of the current-current correlation function $\Lambda$, given in Eq. (7), is valid in the continuous upper complex plane, including the imaginary axis at frequencies different from Matsubara frequencies. One can therefore take the limit $\omega \to 0$ for $\Lambda_{xx}$ either along the real axis, or purely on the imaginary axis, even at finite temperature. Here, we extrapolate the imaginary axis data to obtain the Drude weight without carrying out analytic continuation. This method has earlier been used extensively for calculation of Drude weights in 1D systems [26,27]. In order to carry out the extrapolation to $\omega_n \to 0$, we fit real part of $\Lambda_{xx}(i\omega_n)$ versus $n$ with polynomial and Lorentzian functions. The reason of choosing the Lorentzian is that the current-current correlation function $\Lambda_{xx}(i\omega_n)$ is a well-behaved function on the imaginary axis being the sum of Lorentz curves:

$$\Lambda_{xx}(i\omega_n) = \sum_j c_j \frac{\Delta_j}{\omega_n^2 + \Delta_j^2}. \quad (10)$$

We approximate it by a finite series

$$\Lambda_{xx}(i\omega_n) = \frac{a}{\omega_n^2 + b^2} + \frac{c}{\omega_n^2 + d^2} \quad (11)$$

and determine the constants $a$, $b$, $c$, and $d$. This method, as explained in Ref. [27], is a well-known method for extrapolation of current-current correlation functions and has been extensively used for determining Drude weight at finite temperature for 1D systems. In many cases, a single Lorentzian $a/(b^2 + \omega_n^2)$ provides a good fit to the data. Details of the comparison of the polynomial and Lorentzian fits for various data sets are shown in Appendix A.

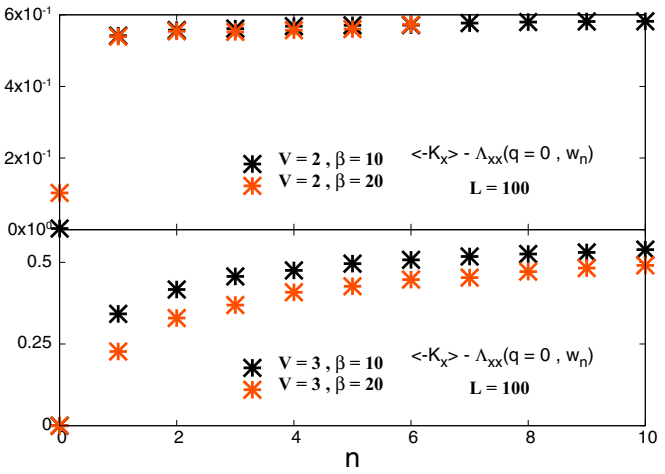


FIG. 1. Results for 1D $t$-$V_1$ model for $V_1 = 2t$ and $3t$. The bottom panel shows the result for $V_1 = 3t$, where $lim_{\omega_n \to 0}[\langle -K_x \rangle - \Lambda_{xx}(i\omega_n)] \to 0$, while this limit gives a nonzero value of $D$ for $V_1 = 2t$ as shown in the top panel.

## III. BENCHMARKING THE CODE

We first calculated the Drude weight for the $t$-$V_1$ model on a 1D chain using SSE and compared our results with the existing literature [26]. For the $t$-$V_1$ model, there is a critical point ($V_{1c}/t = 2$) below which the system is a SF at $T = 0$. For $V_1 > 2t$, the system is an insulator with a CDW order. Though $\rho_s$ is zero at any finite temperature in this 1D system, the Drude weight is finite even at finite temperatures for $V_1 \leqslant 2t$ [26]. In the CDW phase, for $V_1 > 2t$, the Drude weight is zero in the thermodynamic limit at any temperature. Figure 1 shows the response function $\langle -K_x \rangle - \Lambda_{xx}(q = 0, \omega_n)$ vs Matsubara frequency for two values of $V_1$. For $V_1 = 2t$, $\rho_s$ is zero for $T = 0.1t$ (though for $\beta = 20$, for $L = 100$, $\rho_s$ is still nonzero but will tend to zero upon increasing the system size) but for nonzero $\omega_n$ the response function has finite value. The extrapolation of $\langle -K_x \rangle - \Lambda_{xx}(i\omega_n)$ to $\omega_n \to 0$ gives a nonzero Drude weight for this case. On the other hand, for $V_1 = 3t$, as shown in the bottom panel of Fig. 1, the extrapolated value of $\langle -K_x \rangle - \Lambda_{xx}(q = 0, \omega_n)$ goes to zero and also matches with its value at $\omega_n = 0$, implying a zero value for the Drude weight and the stiffness. These results are consistent with published results in Ref. [26] and provide a test to our Drude weight code at low temperature.

Getting reliable Drude weight at higher temperatures, due to the increase in the minimum value of $\omega_m$, is difficult using this method. In order to have an idea about the maximum range of temperatures up to which the extrapolation works, we cross-checked our SSE data against exact diagonalization (ED) results for small system sizes. By calculating the Kubo formula exactly for a small system size in ED where no extrapolation is required to obtain the Drude weight, we could estimate errors in the corresponding SSE calculation of the Drude weight, which requires extrapolation in Matsubara frequency. In exact diagonalization, using the eigenvalues and the eigenvectors, one can calculate the Drude weight from the Lehmann representation of the Kubo formula and one arrives

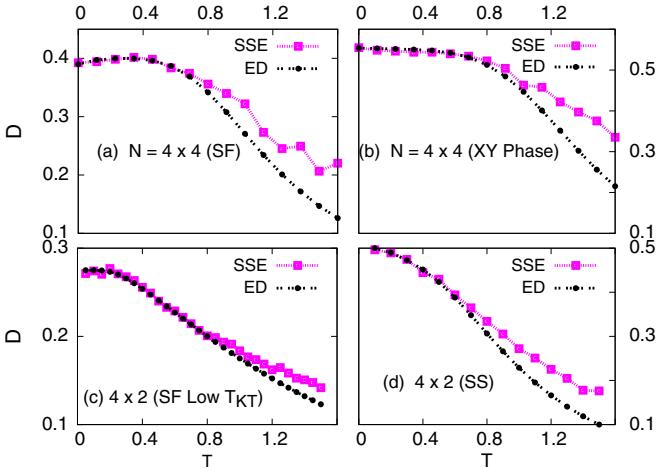


FIG. 2. Comparison of the Drude weight calculated within SSE and ED for small system size in different phases. (a) shows $D$ vs $T$ plots for the results obtained on a $4 \times 4$ lattice for the SF phase in XXZ model. (b) shows the results for the SF in the XY model on a $4 \times 4$ lattice. (c) and (d) shows comparison on a $4 \times 2$ lattice for the low $T_{KT}$ SF phase and the SS-I phase, respectively. Please note that in all the phases, $D_{SSE} - D_{ED} \leqslant 0.01$ for $T \leqslant 0.8 - 1$ in units of $t$.

at the following expressions [25,27]:

$$D(T) = - < K_x > -\frac{2}{L} \sum_{n,m}^{E_n \neq E_m} \frac{p_n}{E_m - E_n} | < n|J_x(0)|m > |^2. \tag{12}$$

Here, $|n\rangle$ is the eigenvector of the Hamiltonian with eigenvalue $E_n$, i.e., $H|n\rangle = E_n|n\rangle$ and $p_n = \exp(-\beta E_n)/Z$ with $Z$ being the partition function. Superfluid stiffness can be calculated as

$$\rho_s(T) = - < K_x > -\frac{2}{L} \sum_{n,m}^{E_n \neq E_m} \frac{p_n}{E_m - E_n} | < n|J_x(0)|m > |^2 - \frac{\beta}{L} \sum_{n,m}^{E_n = E_m} P_n | < n|J_x(0)|m > |^2. \tag{13}$$

As shown in Fig. 2, in all the phases, for $T/t \leqslant 0.8 - 1.0$, $D$ within SSE and ED calculation matches very well.

In the following sections, we present results for $\rho_s$ and $D$ obtained within SSE for various phases realizable in the model in Eq. (1). Details of error in calculation of various physical quantities within SSE are tabulated in Appendix B for different phases studied. The relative error in a physical quantity $A$ is defined as $\Delta A = \frac{\delta A}{\langle A \rangle}$, where $\delta A$ is the standard deviation in $A$ and $\langle A \rangle$ is the average value of A. For the kinetic energy $\langle -K_x \rangle$, $\Delta K_x$ lies between $10^{-2}\%$ to 0.1%. The relative error in the superfluid stiffness $\Delta\rho_s$, for various parameters studied, is in the range 0.5% to 10% and the corresponding error in the response function $\langle -K_x \rangle - \Lambda_{xx}(i\omega_n)$, which is used to obtain the Drude weight, is in the range 0.1% to 10%.

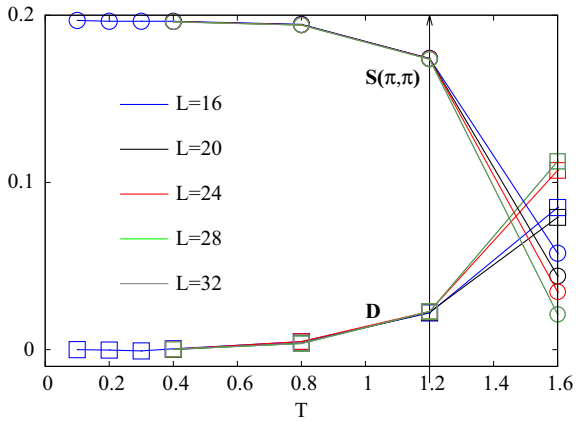


FIG. 3. Structure factor $S(\pi,\pi)$ and the Drude weight $D$ vs $T$, for various system sizes, in the CDW phase. In an insulator, $D$ should be zero at all temperatures. From our SSE calculation, $D \leqslant 0.01$ for $T \leqslant 1.0t$. This gives an idea about the maximum range of temperature up to which our SSE results for $D$ are reliable. Note that error bars for $D$ and $S(\pi,\pi)$ are smaller than the point sizes used (see Appendix B).

## IV. RESULTS IN 2D

In this section, we describe our results for various phases seen in the HCB model in Eq. (1). In order to have an idea about the maximum range of temperature up to which our Drude weight calculation is reliable, we first present our results for the CDW phase followed up by details of other phases.

### A. Drude weight in the CDW Phase

A staggered charge order appears at half-filling in the ground state of model in Eq. (1) for $V_1 = 3t$ and $h = 0$ with no next-nearest-neighbor hopping and repulsion [4]. In terms of the spin model, this phase is equivalent to the antiferromagnetically ordered phase. In terms of bosons, this is a CDW insulator having a gap in the single-particle excitation spectrum. Therefore both superfluid stiffness and the Drude weight must be zero at all temperatures [16].

Figure 3 shows the structure factor $S(\pi,\pi) = \sum_{i,j}(-1)^{i+j}\langle S_z(i)S_z(j)\rangle$, which represents the staggered checkerboard charge order in this system, and the Drude weight $D$ versus $T$ for various system sizes. The CDW order parameter reduces with increase in temperature and goes to zero continuously at a transition temperature of $T_c = 1.5t = 0.5V_1$ [4]. The Drude weight is indeed zero ($D \leqslant 0.01$) up to $T \leqslant 1.0t$ within our SSE calculations. Hence we can say that our results are up to expectations for temperatures below $1.0t$, which is also consistent with benchmarking of our SSE data against ED for small system sizes. Detailed plots of the current-current correlation function $\Lambda_{xx}(i\omega_n)$ versus $\omega_n$ are shown in Fig. 4, along with the kinetic energy values for various temperatures. Notice that for all temperatures shown in Fig. 4, $\lim_{\omega_n \to 0} \Lambda_{xx}(i\omega_n) = \Lambda_{xx}(\omega_n = 0)$, which implies that $D = \rho_s$. Also the extrapolated value of $\Lambda_{xx}(i\omega_n)$ is equal to $\langle -K_x \rangle$, implying that both $D$ and $\rho_s$ are zero in the insulating CDW phase.

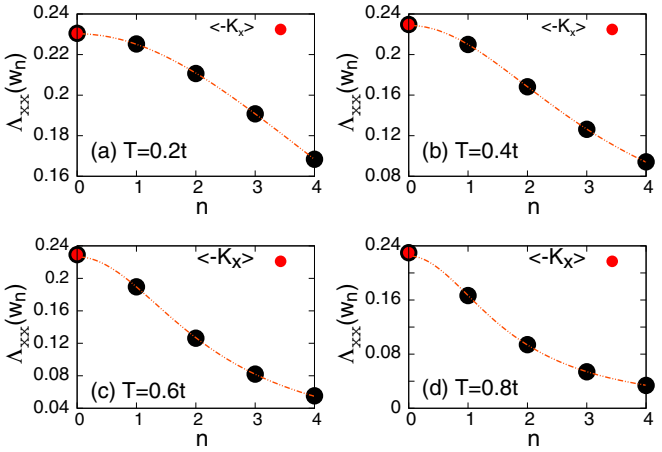


FIG. 4. Extrapolation plots for $\Lambda_{xx}(i\omega_n)$ vs $n$ at various temperatures in the CDW phase. Note that the extrapolated value of $\Lambda_{xx}(i\omega_n)$ is equal to its value at $\omega_n = 0$, implying that $\rho_s = D$. Further, $\Lambda_{xx}(i\omega_n = 0) = \langle -K_x \rangle$, which means both $D$ and $\rho_s$ are zero in the CDW phase. Note that error bars are smaller than the point sizes used (see Appendix B).

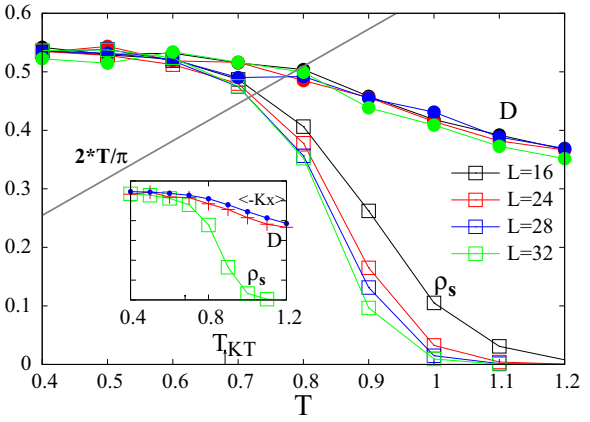


FIG. 5. $\rho_s$ and $D$ vs $T$ for the quantum XY model. The Drude weight $D$ remains nonzero above $T_{\rm KT}$ and shows almost no change with the system size. The inset shows the kinetic energy $\langle -K_x \rangle$, the Drude weight($D$), and superfluid stiffness ($\rho_s$) vs $T$ for $L = 32$. Note that the error bars for $D$, $\langle -K_x \rangle$, and $\rho_s$ are smaller than the point sizes used (see Appendix B).

### B. Superfluid phase

The generic model in Eq. (1) shows a superfluid ground state for a wide range of parameters [4,5,8,9]. The SF phase survives at finite temperature up to $T_{\rm KT}$ where $\rho_s$ goes to zero with a universal drop, of a Kosterlitz-Thouless type transition [20], in the thermodynamic limit. For $T \ll T_{\rm KT}$, where the linear spin wave approximation holds well, $\rho_s \sim D \sim \langle -K_x \rangle$ because the current-current correlation function is vanishingly small. But how the Drude weight behaves at higher temperatures is not known. Our numerical calculation, the results of which are presented in detail below, shows that in all the SF phases, $D = \rho_s$ for $T < T_{\rm KT}$ and for $T > T_{\rm KT}$, $D$ starts deviating from $\rho_s$. For $T \geqslant T_{\rm KT}$, though $\rho_s \to 0$ in the thermodynamic limit, $D$ stays finite even in the thermodynamic limit for a large range of temperatures beyond $T_{\rm KT}$. This implies that for a range of temperatures, the normal phase in this 2D system has dissipationless transport. Note that at very high temperatures, $D$ must go to zero but the temperature at which $D$ goes to zero can not be estimated within our numerical method because the results above $T_{\rm max} = 1.0t$ are not reliable from our calculation.

In order to further confirm our observation about nonzero Drude weight above $T_{\rm KT}$, we analyze the SF phase not only in the pure XY model ($T_{\rm KT} = 0.68t$) but we also looked for the SF phases with a lower $T_{\rm KT}$ because our extrapolation method of evaluating the Drude weight is less erroneous at lower temperatures. Below, we present in detail the results for all the SF phases we have studied.

#### 1. XY model

First, we study the simplest model with only the nearest-neighbor hopping term for hard-core bosons. All other couplings in Eq. (1) are set to zero in this case. In the spin language, this maps to the pure quantum XY model, which has been rigorously studied using SSE [4,5,24] and is known to have a Kosterlitz-Thouless type transition at $T_{\rm KT} = 0.68t$ [21,22].

Figure 5 shows the plot of the superfluid stiffness $\rho_s$, the Drude weight $D$, and the kinetic energy $\langle -K_x \rangle$ vs temperature ($T$) for various system sizes. We see that for $T < T_{\rm KT}$, $\rho_s \sim D$ both being bounded from above by $\langle -K_x \rangle$. For $T > T_{\rm KT}$, though $\rho_s$ goes to zero in the thermodynamic limit, $D$ shows a much slower decrease with $T$. Further, $D$ does not show any significant system size dependence and remains nonzero even in the thermodynamic limit, which implies that the normal phase of this system is an ideal conductor for a range of temperature above $T_{\rm KT}$.

Detailed plots for the current-current correlation function $\Lambda_{xx}(i\omega_n)$ vs $\omega_n$ are shown in Fig. 6. For $T \ll T_{\rm KT}$, deep in the

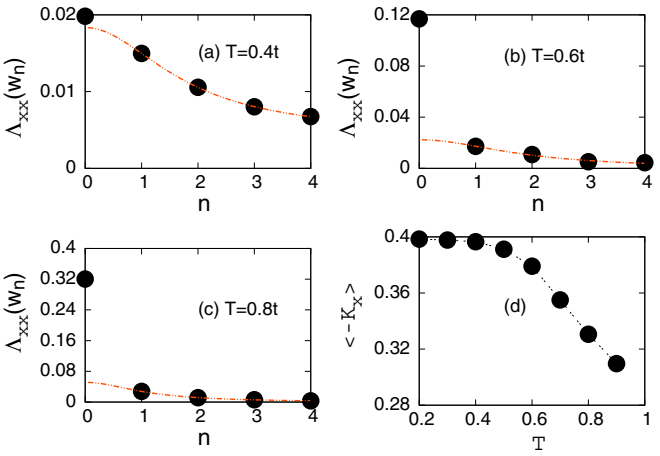


FIG. 6. Extrapolation plots for $\Lambda_{xx}(i\omega_n)$ vs $n$ at various temperatures for XY model for $L = 24$. Note that the extrapolated value of $\Lambda_{xx}(i\omega_n)$ is equal to its value at $\omega_n = 0$ at low temperatures, which implies that $\rho_s = D \sim \langle -K_x \rangle$ at low $T$. However, for higher temperature values, $\lim_{n\to 0} \Lambda_{xx}(i\omega_n) \neq \Lambda_{xx}(\omega_n = 0) \neq \langle -K_x \rangle$, which means that $D \neq \rho_s$ and both of these quantities are different from $\langle -K_x \rangle$. Note that the error bars are smaller than the point sizes used (see Appendix B).

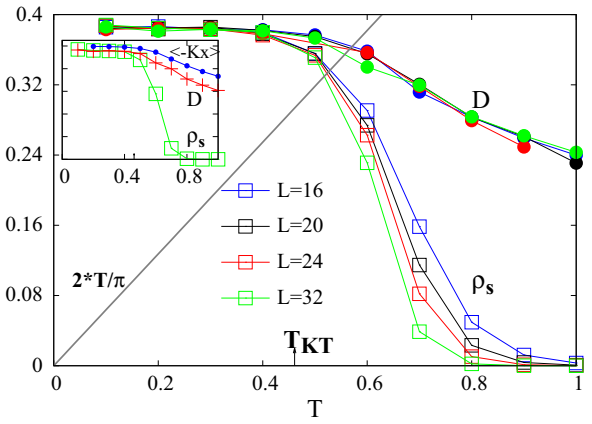


FIG. 7. $\rho_s$ and $D$ vs $T$ for the SF phase of the quantum XXZ model. Results are shown for 2D square lattices of various system lengths ($L$). Inset shows the kinetic energy $\langle -K_x \rangle$, Drude weight($D$) and the superfluid stiffness ($\rho_s$) vs $T$ for $L = 32$. Note that the error bars for $D$, $\langle -K_x \rangle$, and $\rho_s$ are smaller than the point sizes used (see Appendix B).

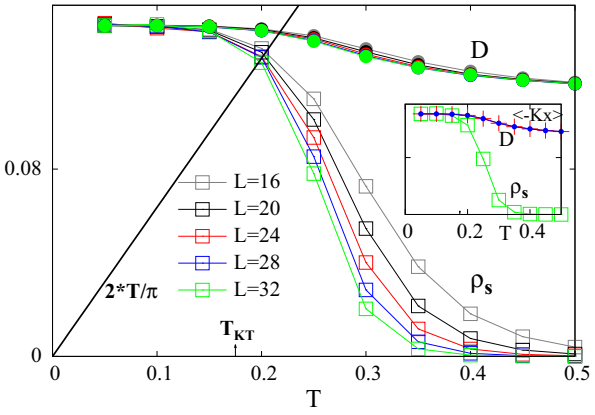


FIG. 8. $\rho_s$ and $D$ vs $T$ evaluated for the low $T_{\rm KT}$ SF phase ($t = 0.9$, $t' = 0.1$, $V_1 = 1$, $V_2 = 4.5$, and $h = 14.0$). Results are shown for 2D square lattices of various lengths ($L$). Inset shows the kinetic energy $\langle -K_x \rangle$, the Drude weight $D$, and the superfluid stiffness ($\rho_s$) vs $T$ for $L = 32$. Note that the error bars in $D$, $\langle -K_x \rangle$, and $\rho_s$ are smaller than the point sizes used.

SF phase, $\lim_{\omega_n \to 0} \Lambda_{xx}(i\omega_n) \sim \Lambda_{xx}(\omega_n = 0) \ll \langle -K_x \rangle$, and thus $D \sim \rho_s$, both being nonzero. As $T$ increases, still being in the SF phase, $\lim_{\omega_n \to 0} \Lambda_{xx}(i\omega_n) < \Lambda_{xx}(\omega_n = 0)$, making $D > \rho_s$. Same trend for $D$ continues for $T > T_{\rm KT}$ where $\Lambda_{xx}(\omega_n = 0) \to \langle -K_x \rangle$ making $\rho_s \to 0$ in the thermodynamic limit. Note that $T_{\rm KT} = 0.68t$ for this phase, which is very close to the $T_{\rm max} = 1.0t$ within which we can get reliable Drude weight. In the following sections, we present results for the SF phases with lower values of $T_{\rm KT}$.

### 2. *XXZ model*

We study another SF phase that is the ground state of the XXZ model with $t = 1$, $V_1 = 3$, and $h = 6$. Here the system shows a KT-type transition at $T_{\rm KT} = 0.47t$, which was concluded from the conventional logarithmic scaling behavior [4] of the transition temperature. In Fig. 7, we show our finite temperature results for $\rho_s$ and $D$ for this phase. It can be clearly seen that at temperatures higher than $T_{\rm KT}$, the Drude weight remains nonzero and shows a slow decreasing behavior with $T$ much like the kinetic energy. Also the system size dependence for $D$ is much weaker compared to that of $\rho_s$ implying a nonzero $D$ even in the thermodynamic limit for a range of temperatures $T > T_{\rm KT}$.

### 3. *Superfluid phase with much lower $T_{\rm KT}$*

We extended our analysis for another superfluid phase, having a much lower transition temperature. We choose various parameters in the Hamiltonian of Eq. (1) to be $t = 0.9$, $t' = 0.1$, $V_1 = 1.0$, $V_2 = 4.5$, and $h = 14.0$ where the system exhibits a superfluid ground state [8]. As shown in Fig. 8, the superfluidity is lost via a Kosterlitz-Thouless type transition at $T_{\rm KT} = 0.17t$. This phase is realized at a particle density of $n = 0.93$, which means holes, the carriers of superfluidity, have very low density 0.07 here. At this low density, neither the hard-core constraint nor the effect of nearest- or next-nearest-neighbor repulsion are significant. Hence the system is in close proximity to an ideal Bose gas in 2D. This is reflected in the low value of $T_{\rm KT}$ and the Drude weight data shown in Fig. 8, which is very close to the behavior of an ideal Bose gas in 2D for which $\rho_s$ is zero at any finite $T$, while the Drude weight $D$ is nonzero being equal to $\langle -K_x \rangle$ [17]. As shown in the inset, for all $T$ studied, $D \sim \langle -K_x \rangle$ for this low-density phase.

As shown in Fig. 8, the Drude weight is equal to $\rho_s$ for $T < T_{\rm KT}$ but stays nonzero for $T > T_{\rm KT}$ without showing any significant system size dependence. Note that since $T_{\rm KT}$ for this system is much smaller than the maximum $T$ limit within which our extrapolation errors are under control, our analysis for $D$ above $T_{\rm KT}$ (up to $T = 0.5t$) is very reliable and supports our proposal of the normal phase being an ideal conductor for a range of temperatures above $T_{\rm KT}$.

After a detailed demonstration of the results for the 2D SF phase, we come to the question why the Drude weight remains nonzero even above $T_{\rm KT}$ where the superfluid stiffness drops to zero in the thermodynamic limit? We propose the following explanation for this observation. There are basically two types of excitations possible in this system, namely, the spin wave excitations and the vortex excitations. This is well known for the corresponding classical model [20] and vortex excitations have also been observed in hard-core bosons [28]. At very low temperature, spin wave excitations are present while the vortex-antivortex pairs are bound, having effectively no vortex excitations. In this regime, $D \sim \rho_s \sim \langle -K_x \rangle$. As $T$ increases, more spin waves are excited and start interacting with each other. For $T \geqslant T_{\rm KT}$, due to unbound vortices, $\rho_s$ drops to zero. However, somehow, $D$ is not suppressed by the presence of vortices. One reason for it might be that the vortices near $T_{\rm KT}$ are ballistic. This hypothesis is made in the original paper by Kosterlitz and Thouless [20]. Another reason might be that the Drude weight, which is obtained from the long-wavelength limit, before taking $\omega \to 0$ limit, of the Kubo formula, does not feel the presence of vortices, which are local excitations though it might be affected by interaction between spin waves

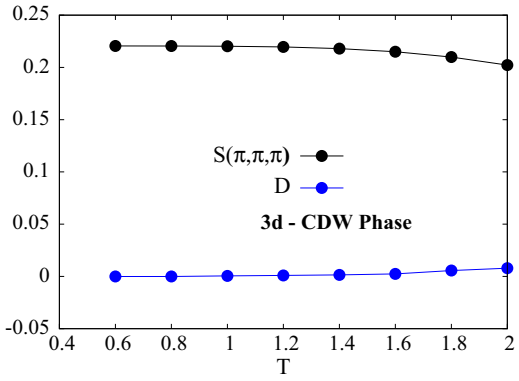


FIG. 9. Temperature dependence of $S(\pi,\pi,\pi)$ and $D$ for the CDW ordered phase in three dimensions for $L = 10$. $D \leqslant 0.01$ for $T < 2t$.

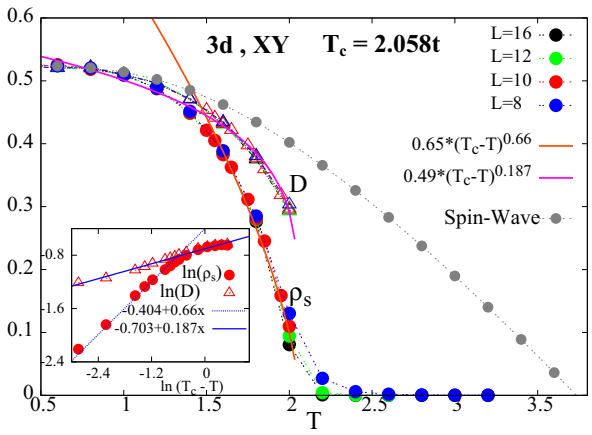


FIG. 10. Temperature dependence of $\rho_s$ and $D$ for a quantum XY model in three dimensions. $\rho_s$ satisfies the scaling form $(T_c - T)^{\nu}$ with $\nu = 0.66$ and $T_c \sim 2.058t \pm 0.01t$. The Drude weight $D$ satisfies the scaling form $D \sim (T_c - T)^{0.187}$ near $T_c$ implying that $D$ goes to zero along with $\rho_s$ at $T_c$. Linear spin wave results, within which $\rho_s = D = \langle -K_x \rangle$, are shown for comparison. Inset shows the fits for $D$ and $\rho_s$ near $T_c$ on the logarithmic scale.

and vortices. This picture, which is only our speculation and is not supported currently by any analytical calculation, can be confirmed by studying the SF phase of HCB's in three dimensions, where the system has true long range order and it undergoes a continuous transition (instead of the KT transition) from the SF phase to the normal phase, having spin waves as the only relevant excitations. With this motivation, we study the quantum XY model on a cubic lattice in the following section and compare results with the 2D case.

## V. RESULTS IN THREE DIMENSIONS

Before presenting our results for the SF phase, we first study the CDW ordered phase in 3D realized for $t = 1.0, V_1 = 3.0$ in Eq. (1) keeping all other couplings to be zero. This will help us in estimating the error bars in the calculation of $D$ and also in finding the maximum temperature up to which the calculation of the Drude weight is reliable for this system. Figure 9 shows the structure factor $S(\pi,\pi,\pi)$ and the Drude weight $D$ versus $T$. It is seen clearly that $D \leqslant 0.01$ for $T \leqslant 2.2t$. Note that in units of bandwidth $W$, which is $4t$ for the square lattice and $6t$ for the cubic lattice, the range of $T$ up to which we get reliable results for $D$ is roughly the same in two and three dimensions.

Now we discuss our results for the quantum XY model in 3D. The temperature dependence of $\rho_s$ and $D$ for various cubes of length $L$, obtained from SSE is shown in Fig. 10. Note that the phase transition in the 3D XY model is in the 3D O(2) class, where the superfluid stiffness goes to zero via a continuous transition at $T_c$. For this universality class, the superfluid stiffness near the transition temperature for $T < T_c$ behaves as $\rho_s \sim (T_c - T)^{(d-2)\nu}$ with $\nu = 0.66$ [23,24]. From the scaling of our SSE data in Fig. 10, we found $T_c = 2.058t \pm 0.01t$, which is close to the value reported earlier [24]. For very low temperature, $D = \rho_s = \langle -K_x \rangle$. This is the regime where the linear spin wave theory works well. As $T$ increases, a deviation from the linear spin wave theory occurs due to the enhanced interaction between spin waves, which is not incorporated in the linear spin wave theory. As a result, $D$ starts deviating from $\rho_s$. In order to see whether $D$ goes to zero at $T_c$ or not, we did fitting of the Drude weight data and found that $D \sim (T_c - T)^{0.187}$ close to $T_c$ as shown in the inset of Fig. 10. Therefore, for a 3D XY model, $D$ goes to zero at $T_c$ along with $\rho_s$ though the critical exponents for $D$ are very different from that of $\rho_s$. This is in clear contrast to the 2D case, where $D$ remains nonzero for a large range of $T$ above $T_{\mathrm{KT}}$. This numerical observation is consistent with our intuitive picture that the Drude weight $D$ is governed primarily by the spin wave excitations and not by the vortex excitations. Before closing the section on results, below, we present our results for an interesting, exotic phase, namely the supersolid phase.

## VI. SUPERSOLID PHASE IN 2D

Finally, we turn our attention towards the supersolid phase defined to be a homogeneous mixture of the superfluid and the CDW phase. In this section, we present results for two types of supersolid phases, which can be realized in the model in Eq. (1).

### A. Supersolid-1

We choose the parameters for the Hamiltonian in Eq. (1) to be $t = 0.9$, $t' = 0.1$, $V_1 = 4.5$, $V_2 = 4.5$, and $h = 9.0$, where the average density for bosons is $2/3$ and a striped SS phase has been reported [8]. The finite temperature phase diagram for this system has not been studied earlier though a similar striped SS phase realized for an almost identical set of parameters has been analyzed at finite temperature [11]. We first study the structure factors corresponding to various charge orderings in this system.

We calculated the structure factor $S(Q) = \sum_{i,j} \exp(i\,Q\,(r_i - r_j))\langle S_z(i)S_z(j)\rangle$ for the ordering wave vector $Q$ along the symmetry directions, namely, $(\pi,0)$, $(0,\pi)$, and $(\pi,\pi)$. Within SSE, it is not possible to calculate $S(\pi,0)$ or $S(0,\pi)$ separately, but one calculates $S_+ = S(\pi,0) + S(0,\pi)$ and $S_- = |S(\pi,0) - S(0,\pi)|$. We found that in the ground state the CDW order breaks the rotational symmetry of the lattice. There is no order along the $(\pi,\pi)$ ordering wave vector

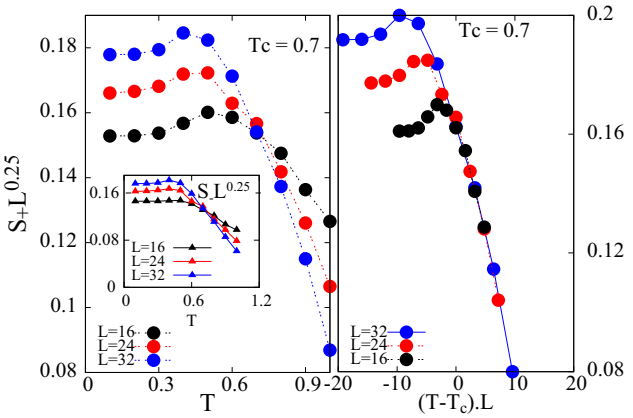


FIG. 11. Structure factors for the CDW order in the SS-I phase. Left panel shows $S_+L^{0.25}$ vs $T$ for various system sizes, while the right panel shows the scaling behavior indicating $T_c \sim 0.7t$. Note that both $S_+$ and $S_-$ are nonzero, as shown in the inset, and of the same strength at all temperatures. This implies the presence of a stripe CDW order either along $x$ or $y$ direction. Note that the error bars for the structure factor are smaller than the point size used (see Appendix B).

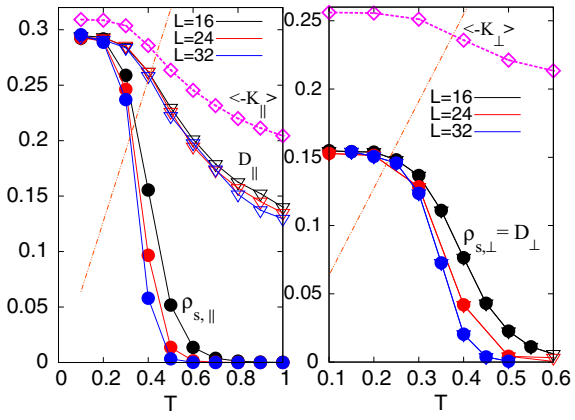


FIG. 12. SSI phase. (Left) $\rho_{s,\parallel}$ and $D_\parallel$ vs $T$ for various system sizes. The behavior is very similar to that of a 2D SF phase where $\rho_s$ drops to zero at $T_{\rm KT}$ while $D$ remains nonzero for a range of $T$ above $T_{\rm KT}$. Note that $\rho_{s\parallel} \sim \langle -K_\parallel \rangle$ at low $T$. (Right) $\rho_{s,\perp}$ and $D_\perp$ vs $T$. Even at very low $T$, $\rho_{s,\perp} \neq \langle -K_\perp \rangle$ due to the coexisting CDW order along this direction. $\rho_{s,\perp} = D_\perp$ at all temperatures and $D_\perp$ goes to zero at $T_{\rm KT}$ along with $\rho_{s,\perp}$. Note that $\langle -K_{\parallel,\perp} \rangle$ has been shown for $L = 16$. The error bars for all quantities are smaller than the point sizes used (see Appendix B).

and $S_+ \sim S_-$, which implies stripe ordering in a system with only one of $S(\pi,0)$ or $S(0,\pi)$ being nonzero. With increase in temperature $T$, both $S_\pm$ remain constant to certain extent for low $T$ and then start decreasing with $T$ as shown in the left panel of Fig. 11. We noticed a slight increase in $S_+$ before it starts decreasing with $T$, which might be due to the presence of a small competing order like $S(\pi,\pi) \ll S_\pm$, although very small yet nonzero in finite size systems. To get an estimate of the transition temperature $T_c$ at which the CDW order is lost due to thermal fluctuations, we did scaling (shown in the right panel of Fig. 11) of $S_\pm$ assuming that the system belongs to the 2D Ising class [11] and undergoes a second-order transition. The estimated value for the transition temperature is $T_c \sim 0.7t$.

This system also has a nonzero superfluid stiffness as shown in Fig. 12. Since the charge order breaks the rotation symmetry, the superfluid stiffness along $x$ and $y$ directions of the lattice are different, that is, $\rho_{s,x} \neq \rho_{s,y}$. The rotation symmetry is broken randomly in different SSE runs, that is, either $S(\pi,0)$ or $S(0,\pi)$ dominates and the superfluid flows only through the channels left open by the solid order. Therefore we calculate the superfluid densities parallel ($\rho_{s,\parallel}$) and perpendicular ($\rho_{s,\perp}$) to the stripe direction as shown schematically in Fig. 13. $\rho_{s,\parallel}(\rho_{s,\perp})$ is calculated for each configuration from the winding numbers in either the $x$ ($y$) or $y$ ($x$) direction depending on whether $S(0,\pi)$ is larger or smaller than $S(\pi,0)$ [29]. Similarly, we calculated the Drude weight parallel $D_\parallel$ and perpendicular $D_\perp$ to the stripe direction from the $\omega \to 0$ limit of the response function $\langle -K_{\parallel,\perp} \rangle - \Lambda_{\parallel,\perp}(i\omega_n)$. Here, $\langle -K_\parallel \rangle - \Lambda_\parallel$ is calculated for each configuration from $\langle -K_x \rangle - \Lambda_{xx}$ or $\langle -K_y \rangle - \Lambda_{yy}$ depending upon whether $S(0,\pi)$ is larger or smaller than $S(\pi,0)$.

For a similar striped SS phase, superfluidity has been shown to be lost via a Kosterlitz-Thouless type transition [11] in spite of the coexisting long-range Ising-type charge order. It was shown that intersection values of $\rho_s(T^\star) = \frac{2T^\star}{\pi}$ for different system sizes follow the logarithmic correction $T^\star = T_{\rm KT}[1 + 1/(2\ln(L/L_0)]$. This indicates weak coupling between XY field and the Ising order because for a situation where the two fields are strongly interacting, the nature of the transition is expected to change [6]. From Fig. 12, the KT transition temperature for the SF order is estimated to be around $T_{\rm KT} \sim 0.28t$.

The left panel in Fig. 12 shows $\rho_{s,\parallel}$ and $D_\parallel$ vs $T$ for various system sizes and the right panel shows the corresponding data for the perpendicular components. For the direction parallel to the stripes, the system behaves very similar to the 2D SF. For $T \ll T_{\rm KT}$, $\frac{|(D_\parallel \sim \rho_{s,\parallel}) - \langle -K_\parallel \rangle|}{\langle -K_\parallel \rangle} \leqslant 6\%$, which is consistent with the linear spin wave approximation within which $\rho_s \sim D \sim \langle -K_x \rangle$ (due to vanishingly small contribution from $\Lambda$). But in the direction perpendicular to the stripes, the response is far from the linear spin wave approximation even at the lowest temperatures, which is reflected in $\frac{|(D_\perp = \rho_{s,\perp}) - \langle -K_\perp \rangle|}{\langle -K_\perp \rangle} \sim 48\%$ for $T \ll T_{\rm KT}$. As we increase $T$ above $T_{\rm KT}$, $D_\parallel$ shows a very slow decrease with $T$ following $\langle -K_\parallel \rangle$ and remains nonzero even

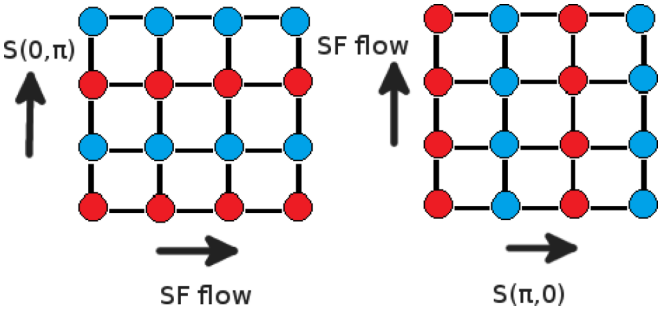


FIG. 13. Schematic figure to show possible stripe CDW order in the SS-I phase and the direction of SF flow in each case.

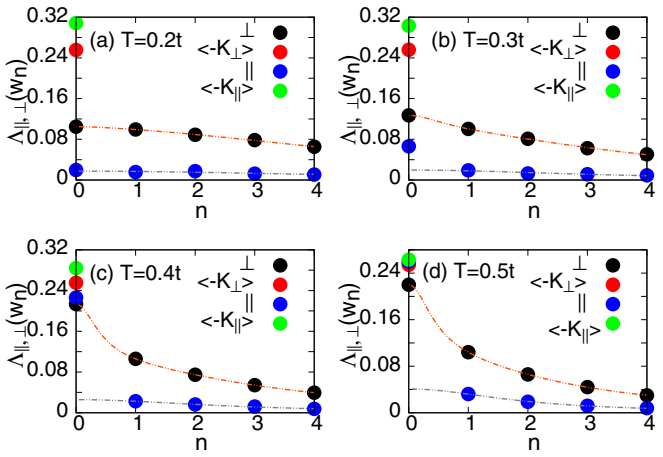


FIG. 14. Extrapolation plots for $\Lambda(i\omega_n)$ in the direction parallel and perpendicular to the stripes, at various temperatures for $L = 16$ in the SS-I phase. At low $T$, the extrapolated value of $\Lambda_{\parallel,\perp}(i\omega_n)$ is equal to its value at $\omega_n = 0$, and thus $\rho_{s,\parallel} = D_\parallel$ and $\rho_{s\perp} = D_\perp$, both being different from the value of the corresponding kinetic energy $\langle -K_{\parallel,\perp}\rangle$. At higher temperature, $\lim_{n\to 0}\Lambda_\parallel(i\omega_n) \neq \Lambda_\parallel(i\omega_n = 0)$, which means that $D_\parallel \neq \rho_{s,\parallel}$. However, $\lim_{n\to 0}\Lambda_\perp(i\omega_n) = \Lambda_\perp(i\omega_n = 0)$ and thus $D_\perp = \rho_{s,\perp}$ even at higher $T$ values. Note that the error bars for the response functions are smaller than the point sizes used (see Appendix B).

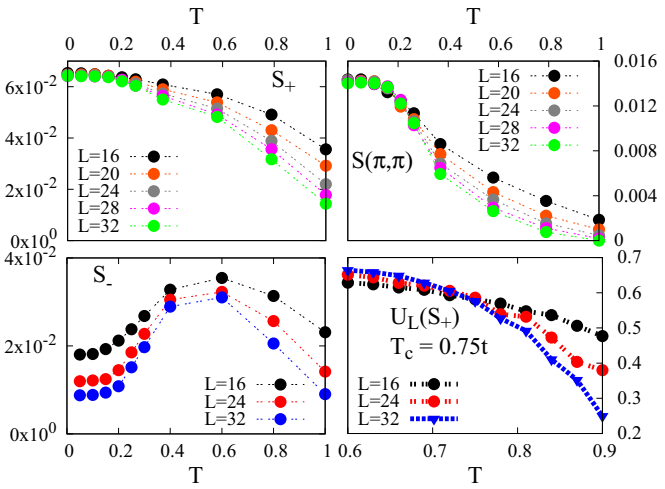


FIG. 15. Structure factors for the SS-II phase as a function of $T$ for various system sizes. Top and bottom panels on the left side show $S_\pm$ vs $T$, respectively, while the top right panel shows $S(\pi,\pi)$ vs $T$ for various system sizes. Binder cumulants for $S_+$ are shown in the bottom right panel, which shows a transition temperature of $T_{cdw} \sim 0.75t$. Note that the error bars for various structure factors are smaller than the point sizes used (see Appendix B).

when $\rho_{s,\parallel}$ has dropped to zero at $T_{\rm KT}$, in complete analogy with other 2D SF phases. However, $D_\perp$ remains equal to $\rho_\perp$ even at higher temperatures and goes to zero at $T_{\rm KT}$ along with $\rho_\perp$. This can be understood in terms of the theorem from Scalapino *et al.* [16], which states that in a system with a nonzero spectral gap $\rho_s = D$. Since in the striped SS phase, CDW order breaks the rotation symmetry (in the thermodynamic limit), the spectral gap must be anisotropic being nonzero along the direction in which CDW order exists.

Detailed plots of the current-current correlation function $\Lambda(i\omega_n)$ in support of this observation are shown in Fig. 14. Notice that $\lim_{\omega_n\to 0}\Lambda_\perp(i\omega_n) = \Lambda_\perp(\omega_n = 0)$ at all temperatures while $\lim_{\omega_n\to 0}\Lambda_\parallel(i\omega_n) < \Lambda_\parallel(\omega_n = 0)$ for $T > T_{\rm KT}$.

Therefore, in the normal phase of this anisotropic SS-I phase, along the direction parallel to the stripes, the system behaves like an ideal conductor for a range of temperatures above $T_{\rm KT}$, while it behaves like an insulator along the direction perpendicular to the stripes for all $T > T_{\rm KT}$.

### B. Supersolid-II

Another SS phase can be realized in the model of Eq. (1) for the set of parameters $t = 0.9$, $t' = 0.1$, $V_1 = 4.5$, $V_2 = 4.5$, and $h = 11.5$, as reported in Ref. [8]. This is a quarter empty star SS phase, which has a ground state characterized by nonzero $S(\pi,\pi)$ and $S_+$ shown as a function of $T$ in Fig. 15 for various system sizes. At $T = 0$, there is a weak anisotropy in the CDW order as it is clear from the very small values of $S_-$ compared to that of $S_+$. Though $S(\pi,\pi)$ and $S_+$ decrease with increasing $T$, the anisotropy parameter $S_-$ increases with $T$ showing its maximum around $T = 0.5t$, though with increasing $L$, $S_-$ prominently decreases as shown in the bottom panel of Fig. 15. To see whether the CDW to normal phase transition is continuous, we calculated the fourth-order Binder cumulant $U(S_+) = 1 - \frac{<O^{+4}>}{3<O^{+2}>^2}$, where $O^+ = \frac{1}{N}\sum_i S_z(i)[\exp(i\pi x_i) + \exp(i\pi y_i)]$ is the order parameter corresponding to the structure factor $S_+$. Here, $(x_i, y_i)$ are coordinates of site $i$. As shown in the right bottom panel of Fig. 15, data for different system sizes cross each other at $T_c = 0.75t$.

After characterizing the CDW order in this phase, we show the finite temperature results for the superfluid stiffness in Fig. 16. Just like in the SS-I phase, here also we

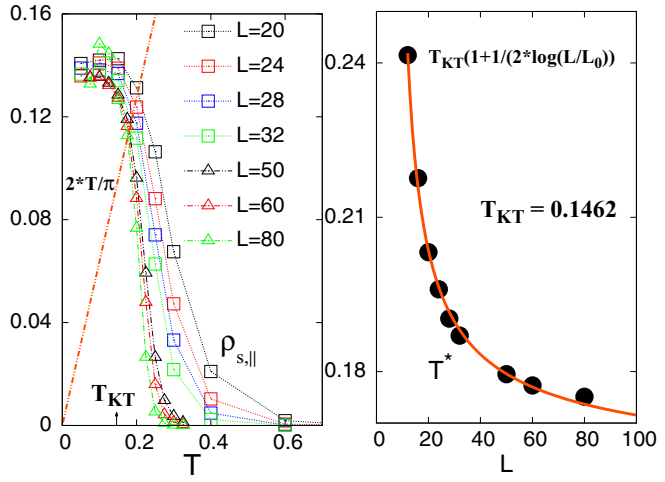


FIG. 16. Left panel shows $\rho_{s,\parallel}$ vs $T$, for the SS-II phase for various system sizes. The point at which the $\rho_{s,\parallel}$ vs $T$ curve crosses $2T/\pi$ gives $T^\star$. Right panel shows $T^\star$ vs $L$, which follows the function $T^\star = T_{\rm KT}[1 + 1/(2\ln(L/L_0))]$ and gives the KT transition temperature to be $T_{\rm KT} = 0.146t$.

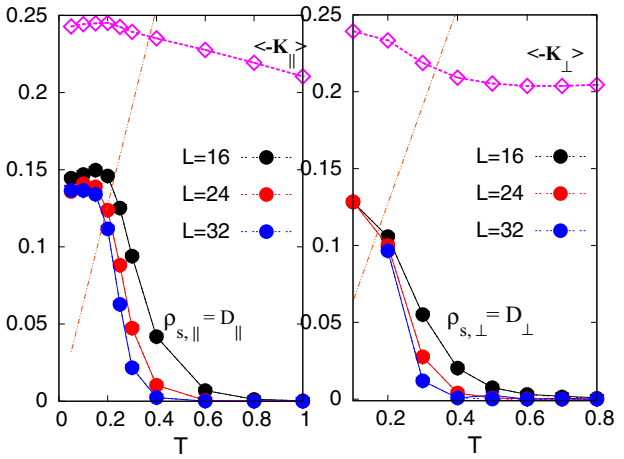


FIG. 17. SS-II phase. (Left) $\rho_{s,\parallel}$ and $D_\parallel$ vs $T$ for various system sizes and (right) the corresponding perpendicular component. $\langle -K_{\parallel,\perp}\rangle$ has been shown for $L = 16$. At all values of $T$, $\rho_s = D$ along both directions. However, even at low temperature, $D_{\parallel,\perp} \neq \langle -K_{\parallel,\perp}\rangle$ due to the coexisting CDW order in this system. Both $\rho_{s,\parallel/\perp}$ and $D_{\parallel/\perp}$ drop to zero at $T_{\rm KT} \sim 0.146t$. The error bars are smaller than the point sizes used (see Appendix B).

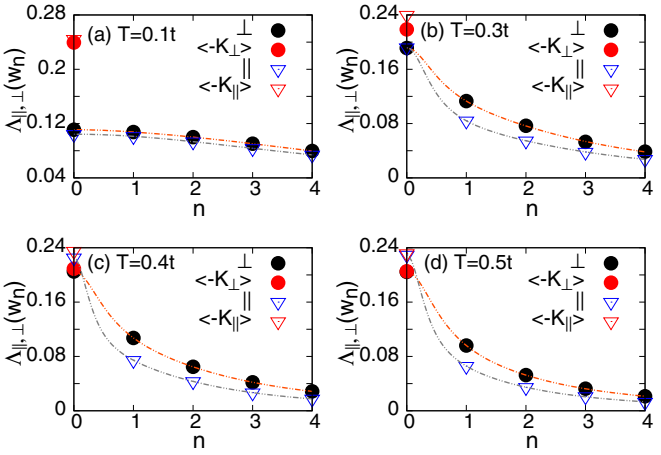


FIG. 18. Extrapolation plots for $\Lambda_{\parallel,\perp}(i\omega_n)$ vs $n$ at various temperatures in the SS-II phase for $L = 16$. For all values of $T$, the extrapolated value of $\Lambda_{\parallel,\perp}(i\omega_n)$ is equal to its value at $\omega_n = 0$, implying that $\rho_s = D$ along both directions. At low $T$, both are different from the value of the corresponding kinetic energy $\langle -K_{\parallel,\perp}\rangle$. For $T > T_{\rm KT}$, the extrapolated values of $\Lambda_{\parallel,\perp}(i\omega_n)$ start approaching $\langle -K_{\parallel,\perp}\rangle$. Hence both, the stiffness $\rho_s$ and $D$ are zero for $T > T_{\rm KT}$. Note that the error bars are smaller than the point sizes used (see Appendix B).

calculate $\rho_{s\parallel}$ and $\rho_{s,\perp}$ for different configuration from the winding numbers in $x$ and $y$ directions depending on whether $S(0,\pi)$ is larger or smaller than $S(\pi,0)$. Plotting $\rho_{s,\parallel}$ as a function of $T$, the intersection values of $\rho_{s\parallel}(T^\star) = \frac{2T^\star}{\pi}$ for different system sizes follow the logarithmic correction $T^\star = T_{\rm KT}[1 + 1/(2\ln(L/L_0))]$ as shown in the right panel of Fig. 16 giving $T_{\rm KT} = 0.146t$. The KT nature of the transition again indicates weak coupling between the XY field and the Ising order because for a situation where the two fields are strongly interacting, the nature of the transition is expected to change [6]. We expect the same physics to hold for the superfluid order along the perpendicular direction.

Finally, we calculate the Drude weight $D_\parallel$ and $D_\perp$ just like in the SS-I phase. As shown in Fig. 17, $D_\parallel = \rho_{s,\parallel}$ and $D_\perp = \rho_{s,\perp}$ at all values of $T$. This happens because $\lim_{\omega_n\to 0} \Lambda_{\parallel,\perp}(i\omega_n) = \Lambda_{\parallel,\perp}(\omega_n = 0)$ at all temperatures as shown in Fig. 18. However, even at very low $T$ due to the coexisting CDW order, $\rho_{s,\parallel} \neq \langle -K_\parallel\rangle$ and the same is true for the perpendicular component. With increase in $T$, the anisotropy in the CDW order increases and it is reflected in the values of $\rho_{s,\parallel}$ and $\rho_{s,\perp}$ being slightly different. Along both directions, both $D$ and $\rho_s$ drop to zero in the thermodynamic limit for $T \geqslant T_{\rm KT}$. Therefore the normal phase of the SS-II phase is not an ideal conductor.

## VII. CONCLUSIONS AND DISCUSSIONS

We calculated the finite temperature Drude weight for the superfluid and the supersolid phases realized in a system of hard-core bosons. The Drude weight and the superfluid stiffness can be obtained from different limits of the Kubo formula. Generally in a metal, $\rho_s = 0$ while $D \neq 0$ at zero temperature. In an insulator, both $\rho_s$ and $D$ are zero while in a superfluid $\rho_s = D \neq 0$ at zero temperature. At any temperature below the transition temperature of the superfluid, $D$ remains nonzero resulting in nondissipative transport and is believed, conventionally, to go to zero for temperatures above the transition temperature. The question we are asking is, in a SF or a SS phase, are these two quantities always equal at all temperatures or can they differ from each other? Is it possible to have a dissipationless ideal conductor of interacting bosons where $\rho_s$ is zero but $D$ is nonzero? In the extended XXZ model of Eq. (1), we calculated the $\rho_s$ and $D$ using SSE. We found that in 2D, in a superfluid phase, at very low temperatures $\rho_s = D = \langle -K_x\rangle$. As $T$ increases, $D$ starts deviating from $\rho_s$. Above $T_{\rm KT}$, $\rho_s$ drops to zero in the thermodynamic limit, but $D$ remains nonzero, decreasing much slowly with $T$ compared to $\rho_s$, for a range of temperatures above $T_{\rm KT}$. Thus for a range of temperatures, the normal phase of a superfluid in this system is an ideal conductor. We confirmed this interesting observation by analyzing various SF phases, specially those for which $T_{\rm KT}$ is small so that our calculation of $D$ is reliable. What is the temperature at which $D$ will go to zero can not be determined from our method because the extrapolation error becomes large with $T$.

Although we do not have full microscopic explanation for this surprising observation, we speculate that it is related to the nature of the Kosterlitz-Thouless transition. Vortex excitations suppress $\rho_s$ making it to drop to zero at $T_{\rm KT}$, but these excitations do not have a significant effect on $D$. Therefore $D$ remains nonzero even above $T_{\rm KT}$ and is basically governed by spin waves only. We further provide support to this speculation by studying the quantum XY model in three dimensions. In the 3D quantum XY model, spin waves are the only relevant excitations that make $\rho_s$ to go to zero continuously at $T_c$. From our calculation, we saw that $D$ obtained from SSE follows the scaling form $(T_c - T)^{0.187}$ and goes to zero at $T_c$ along with $\rho_s$. Thus though the normal phase of a 2D SF is an ideal conductor

for a range of temperatures, it is not true for the normal phase of a 3D SF.

We also studied the exotic supersolid phases in 2D where there is a coexistence of the superfluidity and the CDW order. In the SS-I phase, there is a striped CDW order which breaks the rotational symmetry. Here in the normal phase, for a range of temperatures above $T_{\rm KT}$, the system is an ideal conductor along the direction parallel to the stripes. However, along the direction perpendicular to the stripes, the system is an insulator for all $T > T_{\rm KT}$. In the other SS phase we studied, there is a CDW order along both directions. In this case, we saw that $D = \rho_s$ along both directions and both drop to zero at $T_{\rm KT}$ due to the coexisting CDW order. Thus the normal phase of this SS is not an ideal conductor.

There are deeper questions to be answered in this context, like what makes the Drude weight nonzero in the normal phase of a 2D SF? Typically, in a metal, Drude weight vanishes at finite temperature because the delta function part in $\sigma$ gets broadened due to thermal fluctuations. Exceptions are integrable or near integrable one-dimensional systems [26,27,30] where the Drude weight can remain finite even at finite temperature either due to conserved currents in the system or a part of the current operator has a finite overlap with one of the local conserved quantities, though recently there have been numerical studies on one-dimensional nonintegrable systems, where the current operator has overlap with nontrivial quasilocal conserved quantities, showing nonzero Drude weight [31]. The system we studied is far from being integrable. In an SF phase, $D$ is expected to be nonzero at finite temperatures below the transition temperature. In our results, we found surprisingly that even for a range of temperatures above the transition temperature, $D$ remains nonzero in a 2D SF. Therefore it will be interesting to find out what is the temperature scale at which the Drude weight goes to zero in this 2D SF. It will also be useful to do a vortex dynamic study to understand why vortices can not suppress the Drude weight to zero at $T_{\rm KT}$ and to calculate the Drude weight for other models (e.g., Bose Hubbard model) in two and three dimensions to see if the normal phase in 2D has dissipationless transport above $T_{\rm KT}$. These are questions for future work.

## ACKNOWLEDGMENTS

A.G. like to acknowledge Assa Auerbach, Achim Rosch, and Subroto Mukerjee for comments on this work. We thank P. K. Mohanty for useful discussions and Abhik Basu for suggestions on the manuscript. We are also thankful to the anonymous referee whose critical comments helped in improving the quality of this manuscript.

## APPENDIX A

In this Appendix, we provide details about the fitting of current-current correlation function $\Lambda_{xx}(i\omega_n)$. In Fig. 19, we have shown four different fits using following functions:

$$f1(x) = a + b*x + c*x^2, \tag{A1}$$

$$f2(x) = a + b*x + c*x^2 + d*x^3, \tag{A2}$$

$$f3(x) = a/(b + x^2), \tag{A3}$$

$$f4(x) = a/(b + x^2) + c/(d + x^2). \tag{A4}$$

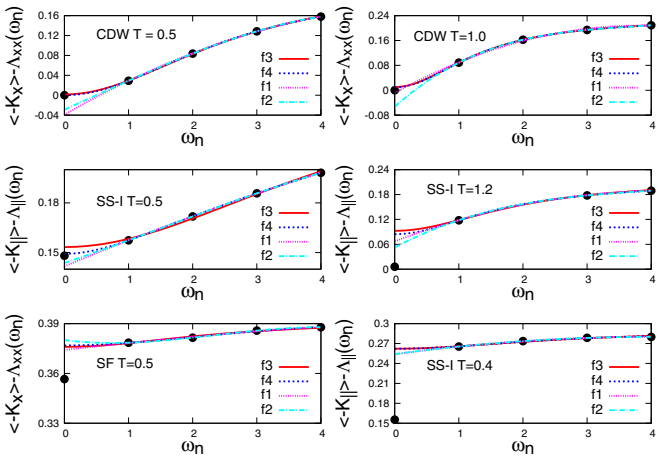


FIG. 19. $< -K_x > -\Lambda_{xx}(i\omega_n)$ vs $n$ for the CDW and the SF phases for $L = 16$ at various temperatures. For the SS-I and SS-II phase, $\langle -K_\parallel \rangle - \Lambda_\parallel(i\omega_n)$ has been shown. (Top) Results for the CDW phase where $D$ must be zero at any value of temperature. Here, the Lorentzian provides the best fit to the data and also the physically correct value of $D = 0$. The polynomial fit at low $T$ in fact gives a negative value of $D$. Similarly, in the SF phase shown in the bottom most left panel, the polynomial fit gives an unphysical uprise in $\langle -K_x \rangle - \Lambda_{xx}(i\omega_n)$ near $n = 0$ and hence is not acceptable.

Note that as we know $\langle -K_x \rangle$, in functions $f1$ and $f2$, $a = \langle -K_x \rangle$. We first look at the fits for the CDW insulating phase where the answer is known to be $D = 0$ at all temperatures. As shown in the top panel of Fig. 19, the Lorentzian provides the best fit of the data obtained from SSE. At $T = 0.5t$, both $f3(x)$ and $f4(x)$ are equally good fits while polynomial functions result in a negative value of $D$. At $T = 1.0t$, $f4(x)$ provides the best fit and again the polynomial fits result in negative values of the Drude weight.

In the middle panel of Fig. 19, results for the SS phase are shown. At $T = 0.5t$, $f4(x)$ provides the best fit. At $T = 1.2t$, also $f4(x)$ works well. In the bottom most panel of Fig. 19, results for the SF phase are shown in the left figure. Here the polynomial fit of degree 3 gives unphysical uprise in $\langle -K_x \rangle - \Lambda_{xx}(i\omega_n)$ in the small $\omega_n$ regime while a polynomial of degree 2 gives a result very close to what one gets from two Lorentzian fits.

## APPENDIX B

In this Appendix, we provide error estimates in the calculation of various physical quantities using SSE. For a physical quantity $A$, we provide tables below for its average value and the standard deviation $\delta A$ obtained from SSE for $L = 16$ at various temperatures and in different phases studied.

*Kinetic energy and superfluid stiffness.* The table below shows the error in the calculation of the kinetic energy $\delta K$ and the superfluid density $\delta\rho_s$ within SSE at various temperatures for XY, SS-I, and SS-II phases. For the SS-I and SS-II phases, the error in the calculation of $< -K_\parallel >$ and $\rho_{s,\parallel}$ has been shown.

| Phase | Temperature (T) | $\langle -K_x \rangle$ | $\delta K_x$ | $\rho_s$ | $\delta\rho_s$ |
|---|---|---|---|---|---|
| XY | 0.4 | 0.5463 | $4.09 \times 10^{-5}$ | 0.5359 | 0.0029 |
| | 0.6 | 0.5379 | $5.45 \times 10^{-5}$ | 0.5216 | 0.0020 |
| | 0.8 | 0.5101 | $9.65 \times 10^{-5}$ | 0.4064 | 0.0041 |
| | 1.0 | 0.4450 | $1.02 \times 10^{-4}$ | 0.1051 | 0.0019 |
| | 1.2 | 0.3852 | $1.08 \times 10^{-4}$ | 0.0078 | 0.0003 |
| Phase | Temperature (T) | $-\langle K_\parallel \rangle$ | $\delta K$ | $\rho_{s,\parallel}$ | $\delta\rho_s$ |
| SS-I | 0.2 | 0.3090 | $1.17 \times 10^{-4}$ | 0.2916 | 0.0018 |
| | 0.4 | 0.2891 | $1.35 \times 10^{-4}$ | 0.1554 | 0.0009 |
| | 0.6 | 0.2475 | $2.18 \times 10^{-4}$ | 0.0136 | 0.0002 |
| | 0.8 | 0.2206 | $1.92 \times 10^{-4}$ | 0.0012 | 0.00005 |
| | 1.0 | 0.2042 | $1.88 \times 10^{-4}$ | 0.0001 | 0.00001 |
| Phase | Temperature(T) | $\langle -K_\parallel \rangle$ | $\delta K$ | $\rho_{s,\parallel}$ | $\delta\rho_s$ |
| SS-II | 0.2 | 0.2494 | $3.23 \times 10^{-4}$ | 0.1459 | 0.001 |
| | 0.4 | 0.2393 | $2.62 \times 10^{-4}$ | 0.0418 | 0.0003 |
| | 0.6 | 0.2295 | $2.78 \times 10^{-4}$ | 0.0069 | 0.0001 |
| | 0.8 | 0.2205 | $1.99 \times 10^{-4}$ | 0.0010 | 0.00004 |
| | 1.0 | 0.2111 | $1.24 \times 10^{-4}$ | 0.0002 | 0.00002 |

*Error estimates for* $\langle -K_x \rangle - \Lambda_{xx}(i\omega_n)$. Below, we give the error estimates (within parenthesis) for the response function $\langle -K_x \rangle - \Lambda_{xx}(i\omega_n)$ obtained from SSE calculations for various values of $T$ and $n$. Again, for the SS-I and SS-II phases, the response function in the direction parallel to the stripes is shown.

*Error estimates for the structure factor*. Here we give details of the error in the calculation of the structure factors in the CDW and the SS phases. In the table below, for each case, the average value of the structure factor is given followed by the error in its calculation within parentheses.

| Phase: | SS-II | | |
|---|---|---|---|
| T | $n = 1$ | $n = 2$ | $n = 3$ |
| 0.2 | $0.1649(8.53 \times 10^{-4})$ | $0.1819(6.76 \times 10^{-4})$ | $0.1973(1.13 \times 10^{-3})$ |
| 0.4 | $0.1682(7.69 \times 10^{-4})$ | $0.1985(6.23 \times 10^{-4})$ | $0.2141(9.40 \times 10^{-4})$ |
| 0.6 | $0.1735(6.24 \times 10^{-4})$ | $0.2024(6.32 \times 10^{-4})$ | $0.2141(7.99 \times 10^{-4})$ |
| Phase: | SS-I | | |
| T | $n = 1$ | $n = 2$ | $n = 3$ |
| 0.2 | $0.2934(6.78 \times 10^{-3})$ | $0.2935(1.62 \times 10^{-3})$ | $0.2942(1.02 \times 10^{-3})$ |
| 0.4 | $0.2654(7.32 \times 10^{-4})$ | $0.2736(1.05 \times 10^{-3})$ | $0.2785(1.00 \times 10^{-3})$ |
| 0.6 | $0.2131(1.07 \times 10^{-3})$ | $0.2293(6.91 \times 10^{-4})$ | $0.2360(5.06 \times 10^{-4})$ |
| Phase: | SF in XY | | |
| T | $n = 1$ | $n = 2$ | $n = 3$ |
| 0.6 | $0.5287(7.23 \times 10^{-4})$ | $0.5331(3.66 \times 10^{-4})$ | $0.5346(5.02 \times 10^{-4})$ |
| 1.0 | $0.4310(8.17 \times 10^{-4})$ | $0.4403(5.18 \times 10^{-4})$ | $0.4435(6.30 \times 10^{-4})$ |
| Phase: | SF in XXZ | | |
| T | $n = 1$ | $n = 2$ | $n = 3$ |
| 0.4 | $0.3837(8.92 \times 10^{-4})$ | $0.3854(5.35 \times 10^{-4})$ | $0.3888(6.00 \times 10^{-4})$ |
| 0.8 | $0.3058(5.58 \times 10^{-4})$ | $0.3210(3.38 \times 10^{-4})$ | $0.3266(8.22 \times 10^{-4})$ |
| Phase: | CDW | | |
| T | $n = 1$ | $n = 2$ | $n = 3$ |
| 0.4 | $0.0196(1.97 \times 10^{-6})$ | $0.0617(6.49 \times 10^{-5})$ | $0.1032(1.12 \times 10^{-4})$ |
| 0.8 | $0.0631(8.71 \times 10^{-5})$ | $0.1358(1.19 \times 10^{-4})$ | $0.1751(2.12 \times 10^{-4})$ |
| 1.2 | $0.1185(1.73 \times 10^{-4})$ | $0.1858(1.98 \times 10^{-4})$ | $0.2102(2.46 \times 10^{-4})$ |

| Phase: | CDW | | |
|---|---|---|---|
| T | $S(\pi,\pi)$ | | |
| 0.4 | $0.1963(1.22 \times 10^{-5})$ | | |
| 0.8 | $0.1945(2.13 \times 10^{-5})$ | | |
| 1.2 | $0.1742(4.48 \times 10^{-5})$ | | |
| 1.6 | $0.0576(6.16 \times 10^{-4})$ | | |
| Phase: | SS-I | | |
| T | $S(\pi,\pi)$ | $S_+$ | $S_-$ |
| 0.2 | $0.0010(3.26 \times 10^{-6})$ | $0.0764(2.85 \times 10^{-5})$ | $0.0730(1.36 \times 10^{-4})$ |
| 0.4 | $0.0011(1.10 \times 10^{-5})$ | $0.0783(2.86 \times 10^{-5})$ | $0.0735(2.53 \times 10^{-4})$ |
| 0.6 | $0.0013(2.01 \times 10^{-5})$ | $0.0793(7.19 \times 10^{-5})$ | $0.0707(5.90 \times 10^{-4})$ |
| 0.8 | $0.0014(2.04 \times 10^{-4})$ | $0.0737(1.12 \times 10^{-4})$ | $0.0606(8.53 \times 10^{-4})$ |
| Phase: | SS-II | | |
| T | $S(\pi,\pi)$ | $S_+$ | $S_-$ |
| 0.2 | $0.0116(1.58 \times 10^{-4})$ | $0.0642(5.54 \times 10^{-5})$ | $0.0212(3.90 \times 10^{-4})$ |
| 0.4 | $0.0077(1.36 \times 10^{-4})$ | $0.0608(5.06 \times 10^{-5})$ | $0.0328(3.53 \times 10^{-4})$ |
| 0.6 | $0.0052(1.16 \times 10^{-4})$ | $0.0570(5.10 \times 10^{-5})$ | $0.0354(3.42 \times 10^{-4})$ |
| 0.8 | $0.0034(6.85 \times 10^{-5})$ | $0.0491(8.43 \times 10^{-5})$ | $0.0313(2.56 \times 10^{-4})$ |


[1] M. P. A. Fisher, P. B. Weichman, G. Grinstein, and D. S. Fisher, Phys. Rev. B **40**, 546 (1989); S. Sachdev, *Quantum Phase Transitions* (Cambridge University Press, Cambridge, 2001), and references therein.

[2] D. Jaksch, C. Bruder, J. I. Cirac, C. W. Gardiner, and P. Zoller, Phys. Rev. Lett. **81**, 3108 (1998); M. Greiner, O. Mandel, T. Esslinger, T. Hansch, and I. Bloch, Nature (London) **415**, 39 (2002); I. Bloch, Nat. Phys. **1**, 23 (2005); I. Bloch, J. Dalibard, and W. Zwerger, Rev. Mod. Phys. **80**, 885 (2008), and references there in.

[3] N. H. Lindner, A. Auerbach, and D. P. Arovas, Phys. Rev. B **82**, 134510 (2010); A. Mihlin and A. Auerbach, *ibid.* **80**, 134521 (2009).

[4] G. Schmid, S. Todo, M. Troyer, and A. Dorneich, Phys. Rev. Lett. **88**, 167208 (2002).

[5] F. Hébert, G. G. Batrouni, R. T. Scalettar, G. Schimd, M. Troyer, and A. Dorneich, Phys. Rev. B **65**, 014513 (2001).

[6] D. Heidarian and K. Damle, Phys. Rev. Lett. **95**, 127206 (2005); M. Boninsegni and N. Prokof'ev, *ibid.* **95**, 237204 (2005).

[7] P. Sengupta, L. P. Pryadko, F. Alet, M. Troyer, and G. Schmid, Phys. Rev. Lett. **94**, 207202 (2005); R. G. Melko, A. Paramekanti, A. A. Burkov, A. Vishwanath, D. N. Sheng, and L. Balents, *ibid.* **95**, 127207 (2005); T. Suzuki and N. Kawashima, Phys. Rev. B **75**, 180502(R) (2007); F. Wang, F. Pollmann, and A. Vishwanath, Phys. Rev. Lett. **102**, 017203 (2009); H. C. Jiang, M. Q. Weng, Z. Y. Weng, D. N. Sheng, and L. Balents, Phys. Rev. B **79**, 020409(R) (2009); H. T. Ueda and K. Totsuka, *ibid.* **81**, 054442 (2010); X.-F. Zhang, Y.-C. Wen, and S. Eggert, *ibid.* **82**, 220501(R) (2010); X.-F. Zhang, R. Dillenschneider, Y. Yu, and S. Eggert, *ibid.* **84**, 174515 (2011); D. Yamamoto, A. Masaki, and I. Danshita, *ibid.* **86**, 054516 (2012); H.-C. Jiang, L. Fu, and C. Xu, *ibid.* **86**, 045129 (2012); T. Mishra, R. V. Pai, and S. Mukerjee, Phys. Rev. A **89**, 013615 (2014).

[8] Y.-C. Chen, R. G. Melko, S. Wessel, and Y.-J. Kao, Phys. Rev. B **77**, 014524 (2008).

[9] K.-K. Ng and Y.-C. Chen, Phys. Rev. B **77**, 052506 (2008).

[10] F. Mila, J. Dorier, and K. P. Schmidt, Prog. Theor. Phys. Suppl. **176**, 355 (2008).

[11] K. Ng, Phys. Rev. B **82**, 184505 (2010).

[12] P. Phillips and D. Delidovich, Science **302**, 243 (2003).

[13] S. Vishveshwara, C. Bena, L. Balents, and M. P. A. Fisher, Phys. Rev. B **66**, 165411 (2002).

[14] S. Doniach and D. Das, Brazillian J. Phys. **33**, 740 (2003).

[15] D. N. Sheng, O. I. Motrunich, and M. P. A. Fisher, Phys. Rev. B **79**, 205112 (2009).

[16] D. J. Scalapino, S. R. White, and S. Zhang, Phys. Rev. B **47**, 7995 (1993).

[17] S. Sorella, AIP Conf. Proc. **816**, 265 (2006).

[18] O. F. Syljuasen and A. W. Sandvik, Phys. Rev. E **66**, 046701 (2002).

[19] A. W. Sandvik, J. Phys. A **25**, 3667 (1992)

[20] V. L. Berezinskii, Sov. Phys. JETP **34**, 610 (1972); J. M. Kosterlitz and D. J. Thouless, J. Phys. C **6**, 1181 (1973); J. M. Kosterlitz, *ibid.* **7**, 1046 (1974).

[21] H. Q. Ding and M. S. Makivic, Phys. Rev. B **42**, 6827 (1990).

[22] K. Harada and N. Kawashima, Phys. Rev. B **55**, R11949(R) (1997).

[23] M. E. Fisher, M. N. Barber, and D. Jasnow, Phys. Rev. A **8**, 1111 (1973).

[24] J. Carrasquilla and M. Rigol, Phys. Rev. A **86**, 043629 (2012).

[25] G. D. Mahan, *Many Particle Physics*, 2nd ed. (Plenum Press, New York, 1990).

[26] D. Heidarian and S. Sorella, Phys. Rev. B **75**, 241104 (2007).

[27] S. Kirchner, H. G. Evertz, and W. Hanke, Phys. Rev. B **59**, 1825 (1999).

[28] E. Loh, Jr., D. J. Scalapino, and P. M. Grant, Phys. Rev. B **31**, 4712(R) (1985).

[29] G. G. Batrouni, R. T. Scalettar, G. T. Zimanyi, and A. P. Kampf, Phys. Rev. Lett. **74**, 2527 (1995); G. Schmidand and M. Troyer, *ibid.* **93**, 067003 (2004); R. G. Melko, A. Del Maestro, and A. A. Burkov, Phys. Rev. B **74**, 214517 (2006).

[30] X. Zotos, F. Naef, and P. Prelovsek, Phys. Rev. B **55**, 11029 (1997); A. Rosch and N. Andrei, Phys. Rev. Lett. **85**, 1092 (2000).

[31] X. Zotos, Phys. Rev. Lett. **82**, 1764 (1999); S. Fujimoto and N. Kawakami, *ibid.* **90**, 197202 (2003); J. Herbrych, P. Prelovsek, and X. Zotos, Phys. Rev. B **84**, 155125 (2011); C. Karrasch, J. Hauschild, S. Langer, and F. Heidrich-Meisner, *ibid.* **87**, 245128 (2013); P. Jung and A. Rosch, *ibid.* **76**, 245108 (2007); C. Karrasch, J. H. Bardarson, and J. E. Moore, Phys. Rev. Lett. **108**, 227206 (2012).